HHS Public Access

Author manuscript

J Invest Dermatol. Author manuscript; available in PMC 2023 March 01.

Published in final edited form as:

J Invest Dermatol. 2022 March ; 142(3 Pt A): 679–691.e3. doi:10.1016/j.jid.2021.04.039.

ONCOSTATIN M IMPROVES CUTANEOUS WOUND RE-EPITHELIALIZATION AND IS DEFICIENT UNDER DIABETIC CONDITIONS

Amitava Das[1], **Amit K. Madeshiya**[1], **Nirupam Biswas**[1], **Nandini Ghosh**[1], **Mahadeo Gorain**[1], **Atul Rawat**[1], **Sanskruti P. Mahajan**[1], **Savita Khanna**[1], **Chandan K. Sen**[1], **Sashwati Roy**[1,*]

[1]Department of Surgery, IU Health Comprehensive Wound Center, Indiana Center for Regenerative Medicine and Engineering, Indiana University School of Medicine, Indianapolis, IN, 46202

Abstract

Impaired re-epithelialization characterized by hyperkeratotic non-migratory wound epithelium is a hallmark of non-healing diabetic wounds. In chronic wounds, copious release of oncostatin M (OSM) from wound macrophages is evident. OSM is a potent keratinocyte activator. This work sought to understand the signal transduction pathway responsible for wound-re-epithelialization, the primary mechanism underlying wound closure. Daily topical treatment of full-thickness excisional wounds of C57bl/6 mice with recombinant murine OSM improved wound re-epithelialization and accelerated wound closure by bolstering keratinocyte proliferation and migration. OSM activated the JAK-STAT pathway as manifested by STAT3 phosphorylation. Such signal transduction in the human keratinocyte induced TP63, the master regulator of keratinocyte function. Elevated TP63 induced integrin beta 1, a known effector of keratinocyte migration. In diabetic wounds, OSM was more abundant compared to the level in non-diabetic wounds. However, in diabetic wounds OSM activity was compromised by glycation. Aminoguanidine, a deglycation agent, rescued compromised keratinocyte migration caused by glycated OSM. Finally, topical application of recombinant OSM improved keratinocyte migration and accelerated wound closure in db/db mice. This work recognizes that despite its abundance at the wound-site, OSM is inactivated by glycation and topical delivery of exogenous OSM is likely to be productive in accelerating diabetic wound closure.

[*]**Address correspondence to:** Sashwati Roy, PhD, 975 W Walnut St, Suite 444, Medical Research Library Building, Indiana University School of Medicine, Indianapolis, IN 46202. Tel. 317 278 2706, roysa@iu.edu.

AUTHOR CONTRIBUTIONS

Conceptualization, S.R., C.K.S. and A.D.; Methodology, A.D., S.K., S.R. and C.K.S.; Investigation and Validation, A.D., A.M., N.B., N.G., M.G., A.R., S.P.M., S.K.; Formal Analysis, A.D., A.M., N.B., N.G., M.G., A.R., S.P.M., S.K., S.R. and C.K.S.; Writing, S.R., C.K.S. and A.D.; Visualization, A.D., S.R., A.M., N.B., and N.G.; Funding Acquisition, C.K.S, S,R.; Resources, C.K.S. and S.R.; Supervision, C.K.S. and S.R.

CONFLICT OF INTEREST: The authors declare no conflict of interest.

Keywords

OSM; re-epithelialization; diabetes; p63; integrin; glycation

Introduction

The interleukin (IL)-6 family cytokines is responsive to inflammatory processes such as the acute-phase reaction, tissue damage, and infection(Gadient and Patterson, 1999). Oncostatin M (OSM) is a pleiotropic cytokine that belongs to this family. OSM binds to the heterodimeric OSM receptor (OSMR). Formation of this heterodimeric complex activates several signaling cascades of which Janus kinase (JAK)s represent a major path(Houben et al., 2019). Upon activation JAKs recruit signal transducer and activation transcription (STAT)s(Houben et al., 2019). STATs function as latent transcription factors that are phosphorylated by activated JAKs(Houben et al., 2019). Phosphorylated STATs translocate to the cell nucleus and bind to specific DNA sequences in promoters or to other transcription factors to modulate gene expression(Houben et al., 2019). OSM regulates epithelial function in a wide range of pathophysiological settings including tumor as well as non-tumor biology(Beigel et al., 2014, Boniface et al., 2007, Canady et al., 2013, Jorcyk et al., 2006, Sterbova et al., 2018). For example, OSM mediates STAT3-dependent intestinal epithelial restitution(Beigel et al., 2014). OSM increases cell migration in a variety of cell types including normal human epidermal keratinocytes(Boniface et al., 2007, Canady et al., 2013).

Impairment of cutaneous wound healing is a debilitating complication commonly encountered during diabetes mellitus(Das et al., 2016, Singh et al., 2019). Understanding of the molecular mechanisms underlying impairment in keratinocyte function at the diabetic wound-edge is thus warranted. OSM is a potent keratinocyte activator(Boniface et al., 2007, Shin et al., 2014).We have reported that OSM is a key cytokine abundantly produced by human wound-site macrophages(Ganesh et al., 2012). In non-diabetic wounds OSM improved wound closure during the early inflammatory phase of healing *via* a PGE2-Axl pathway(Ganesh et al., 2012). In this work we sought to characterize the underlying mechanisms by which the OSM pathway fails under conditions of diabetes with the aim to inform rescue strategies.

Results

OSM treatment facilitates wound closure by improving re-epithelialization

A splinted full-thickness excisional murine wound model was employed to test the significance of OSM in wound healing *in vivo*. Daily topical treatment of such wounds with recombinant murine OSM accelerated the wound closure as noted from initial phase (d3 post-wounding) to late phase (d13 post-wounding) (Fig. 1a,b). OSM-treatment resulted in complete closure of the wounds on d13 post wounds as compared to vehicle-treated wounds that remained open at that time-point (Fig. 1b). Successful delivery of OSM to the d13 wound-edge tissue was verified using ELISA (Fig. 1c). Exogenous OSM accelerated wound closure and improved wound re-epithelialization (Fig. 1d,e). The significance of

OSM on wound-edge keratinocyte proliferation and migration, two processes required for wound re-epithelialization, was tested. Ki67 is a marker for proliferative cells that are primarily present in the basal region of the wound epithelium(Biswas et al., 2010). Integrin beta 1 (ITGB1) is directly implicated in keratinocyte migration and wound re-epithelialization(Grose et al., 2002, Koivisto et al., 2014). OSM treatment induced wound-edge keratinocyte proliferation as observed by increased abundance of $Ki67^+$ cells (Fig. 1f,g). The d3 wound-edge epithelium was captured using laser capture microdissection (LCM) (Fig. 1h) followed by determination of *Itgb1* mRNA expression using quantitative RT-PCR. OSM induced *Itgb1*expression in laser captured d3 wound-edge keratinocytes compared to vehicle treated group (Figs. 1i). Consistent data were obtained using whole wound-edge tissue where ITGB1 protein levels were also higher (Fig. 1j-l). Taken together, these findings support the contention that OSM treatment augmented wound closure and re-epithelialization *via* enhanced wound-edge keratinocyte proliferation and migration.

OSM induces keratinocyte proliferation and migration via a STAT3 ➔p63 pathway.

To gain insight into the molecular mechanisms underlying OSM-mediated enhanced keratinocyte proliferation and migration, cultured human keratinocytes were studied (Fig. S1a). Treatment with exogenous recombinant OSM increased proliferation and migration (Fig. S1b-d). These findings are consistent with results observed in the wound-edge epithelium as well as previous reports on the increased motility of keratinocytes by OSM (Nguyen et al., 2020). p63, also known as TP63, is a master regulator of keratinocyte proliferation(Koster et al., 2007) which positively regulates wound re-epithelialization(Romano et al., 2012). Treatment of keratinocytes with OSM induced both p63 mRNA and protein expression (Fig. 2a-d). Consistent results were obtained in vivo where exogenous OSM treatment was noted to induce p63 mRNA and protein expression in the d3 wound-edge epithelium (Fig. 2e-g).

The wound fluid bathing the wound tissue reflects the wound microenvironment and is rich in OSM(Ganesh et al., 2012). In this work, wound fluid OSM was neutralized with OSM-neutralizing antibody (Fig. 2h; Supplementary Table S1). Treatment of human keratinocytes with 10% (v/v) patient-derived wound fluid significantly induced *p63* mRNA expression in a manner that was attenuated under conditions of neutralization of OSM (Fig. 2i). Using a promoter-reporter assay, it was noted that OSM induces p63 transcriptionally (Fig. 2j, S2). siRNA-mediated knockdown of *p63* (Fig. 2k) resulted in significant attenuation of OSM-induced keratinocyte proliferation and migration pointing towards a significant role of p63 in both processes (Fig. 2l-n). OSM is known to interact with the OSM-specific receptors to turn on signal transduction *via* the JAK/STAT tyrosine kinase pathway(Gomez-Lechon, 1999). In keratinocytes, OSM caused phosphorylation of STAT3 (Fig. 3a). STAT3 was directly implicated in OSM-dependent induction of p63 (Fig. 3b-e).

Knockdown studies were conducted to test the significance of ITGB1 in OSM-induced keratinocyte migration *in vitro*. In human keratinocytes, OSM treatment induced the expression of ITGB1 protein (Fig. 4a,b). The siRNA-mediated knockdown of *ITGB1* (Fig. 4c) significantly attenuated OSM-dependent keratinocyte migration (Fig. 4d,e). Knockdown

of *p63* blunted OSM-dependent expression of ITGB1 protein (Fig. 4f,g). These findings demonstrate that OSM-induced ITGB1 expression is regulated by p63.

Diabetic wounds host abundant yet inactive OSM

OSM has previously been reported to be abundant in human chronic wound fluid(Ganesh et al., 2012). However, the abundance of this cytokine in diabetic wound fluids remains unknown. We report that OSM levels are high in diabetic human wound fluid and murine d5 wound-edge tissue as compared to their non-diabetic counterparts (Fig. 5a,b; Supplementary Table S2). To test its functionality in diabetic wounds OSM was immunoprecipitated from wound-edge tissue followed by immunoblotting with anti-AGE (Advanced Glycation End product) antibody to determine glycation. AGE was highly abundant in OSM derived from d5 diabetic wound-edge tissue as compared to OSM from non-diabetic control wound tissues (Fig. 5c). To test the functional significance of glycated OSM, methylglyoxal (MGO) was used to generate glycated OSM. Significant impairment in OSM-dependent migration was noted in keratinocytes treated with glycated OSM as compared to native OSM. Deglycation of MGO-modified OSM using aminoguanidine rescued its functional activity demonstrating that glycation limits the ability of OSM to induce keratinocyte migration (Fig. 5d-f). Aminoguanidine alone did not significantly modify the keratinocyte cell migration as compared to corresponding control (data not shown). Loss of upstream signal caused by glycation of OSM resulted in lower p63 expression in d5 diabetic wound-edge tissue (Fig. 5g,h). Consistently, the expression of ITGB1 in d5 diabetic wound-edge tissues and keratinocytes were significantly lower (Fig. 5i-k) resulting in impaired re-epithelization in d7 diabetic wounds (Fig. 5l-m).

Topically applied OSM accelerates diabetic wound closure

Hyperglycemia impaired keratinocyte migration in cultured keratinocytes (Fig. S3a,b). OSM treatment rescued hyperglycemia-induced keratinocyte migration impairment (Fig. S4a,b). Compared to vehicle treated diabetic wounds, OSM significantly accelerated wound closure (Fig. 6a,b). Successful delivery of OSM at the diabetic wound-edge was validated (Fig. 6c). The treatment of diabetic wounds with OSM significantly improved wound re-epithelialization (Fig. 6d,e). Under these experimental conditions, p63 (Fig. 6f,g) and ITGB1 expression in the keratinocytes (Fig. 6h-j) were elevated.

Discussion

Inadequate wound closure represents a major complication in diabetes(Das et al., 2016). An orchestrated process involving multiple cell types plays out in a temporally sensitive manner to achieve wound re-epithelialization, a major mechanism underlying wound closure. This work recognizes OSM as an important driver of wound re-epithelialization. To the contrary of what one would expect, OSM is such a factor that is abundant in higher levels both in patient derived wound fluid as well as in murine wound-edge tissue. Such elevated OSM, present under diabetic conditions, exists in a glycated and inactive form. Reversal of such glycation or topical application of native OSM is able to accelerate wound closure in the diabetic. Under hyperglycemic conditions, reducing sugar molecules non-enzymatically react with proteins to produce advanced glycated endproducts (AGE)(Wautier and Schmidt,

2004). Protein glycation takes place by the Maillard reaction in which the carbonyl group of the reducing sugar reacts with the amino group of the protein to form a Schiff's base. The latter undergoes rearrangement to form Amadori product which in turn may undergo further rearrangements and modifications to form irreversible end products(Wautier and Schmidt, 2004). Glycation-induced impairment of protein function is one of the primary mechanisms by which glycation adversely affects living cells(Takahashi, 2015). Loss of function by glycation has been consistently reported in independent studies(Das et al., 2016, Kuzuya et al., 1998, Morita et al., 2005, Peppa et al., 2009). We have previously reported that in diabetic wounds glycation of milk fat globule epidermal growth factor-factor 8 (MFG-E8) compromises its function resulting in impaired clearance of apoptotic cells, persistent inflammation and impaired wound closure(Das et al., 2016). Likewise, glycated collagen hinders migration of keratinocytes(Kuzuya et al., 1998, Morita et al., 2005, Peppa et al., 2009). In this work glycation of OSM impaired its functional activity hindering keratinocyte migration. OSM, rich in arginine and lysine residues, is particularly susceptible to glycation(Ryan et al., 2015). Aminoguanidine is a nucleophilic hydrazine whose presence spares glycation of proteins induced by methylglyoxal(Thornalley, 2003). Aminoguanidine is known to prevents experimental diabetic nephropathy the pathogenesis of which includes protein glycation(Yu and Zuo, 1997). Aminoguanidine-dependent rescue of OSM function and related keratinocyte migration that was affected by methylglyoxal directly implicates involvement of glycation as one of the factors.

Wound re-epithelialization involves cross-talk between resident keratinocytes and visiting wound-site macrophages. Initial evidence in support of this contention came from early studies demonstrating impairment of re-epithelialization under conditions of macrophage ablation(Leibovich and Ross, 1975, Mirza et al., 2009). More recent work from our laboratories provided direct evidence of such cross-talk via transfer of signaling cargo borne by extracellular vesicles(Sinha et al., 2018). Our previous work recognized human wound-site macrophages as a significant source of OSM which appears in the wound fluid(Ganesh et al., 2012). Additionally, neutrophils have also been reported to express OSM at the wound site in the early inflammatory phase(Goren et al., 2006). This work reports a scenario where despite an abundance of OSM at the diabetic wound-site, wound-re-epithelialization is impaired. Identification of the glycation-dependent inactivation of endogenous OSM makes room for a therapeutic strategy of the application of exogenous OSM to accelerate diabetic wound closure.

p63 is a master regulator of epidermal keratinocyte proliferation(Koster and Roop, 2004, Truong et al., 2006) and wound re-epithelialization(Morasso and Tomic-Canic, 2005, Romano et al., 2012). This work directly implicates p63 in supporting keratinocyte migration. This observation is of major functional significance because it is cell migration that is a limiting factor in diabetic wound closure. In such cases, the keratinocytes are known to be hyperproliferative *via* a c-myc pathway causing hyperkeratosis(Pastar et al., 2014, Stojadinovic et al., 2005). As part of the signal transduction pathway of p63 dependent keratinocyte migration, this work recognizes a downstream role of ITGB1. Integrins are major cell surface receptors for epidermal adhesion to the basement membrane and control a wide variety of keratinocyte functions including migration(DiPersio et al., 2016). However, signals immediately upstream of ITGB1 remained unclear. Importantly, loss of ITGB1 in

keratinocytes caused severe defect in wound healing *in vivo* underscoring the significance of this signaling pathway(Grose et al., 2002). Keratinocytes lacking ITGB1 suffered from impaired migration and were more densely packed in the hyperproliferative epithelium, a phenotype consistent with hyperkeratosis observed in clinical cases of impaired healing of diabetic wounds(Pastar et al., 2014, Stojadinovic et al., 2005).

Binding of active OSM to its receptor induces the phosphorylation of STAT3(Fossey et al., 2011). STAT3, a member of the JAK-STAT pathway is known to induce integrin expression(Wooten et al., 2000). This work recognizes the involvement of p63, downstream of STAT3, as a part of the signal transduction pathway by which OSM induces ITGB1. Elucidation of novel molecular mechanisms which are implicated in limiting closure of diabetic wounds are necessary for the development of productive therapeutic strategies. This work recognizes that despite its abundance at the wound-site OSM is inactivated by glycation and that topical delivery of exogenous OSM is likely to be productive in accelerating diabetic wound closure. The chronic wound-site microenvironment is known to be acidic(Gladden, 2004, Hunt et al., 2007) and rich in proteases(McCarty and Percival, 2013). OSM withstands both conditions well. It induces the expression of protease inhibitors(Santamaria et al., 2013). Furthermore, it retains function in an acidic pH for prolonged periods of time(Ryan et al., 2015). These characteristics make approaches involving topical delivery of OSM to the wound-site likely to be productive.

Materials and Methods

Human subjects and fluid collection from chronic wounds

Subjects participating in the study were chronic wound patients undergoing negative pressure wound therapy (NPWT) as part of standard clinical care. Demographic characteristics of patients and wound-related information are presented in Supplementary Table S1 and Supplementary Table S2. The NPWT dressing (sponges) were collected from each patient for cell isolation and wound fluid collection. Wound fluids were derived from NPWT dressing by lavaging the wound dressing with saline solution(Ganesh et al., 2012). All human studies were approved by The Ohio State University Institutional Review Board. Declaration of Helsinki protocols was followed, and patients gave their written informed consent.

Secondary Intention Excisional Murine Dermal Wound Model

All the animal studies were performed in accordance with protocols approved by the Institutional Animal Care and Use Committee of the Ohio State University and Indiana University. Male C57BL/6 mice (age, 8–10 weeks old) were obtained from Harlan Laboratory (Indianapolis, IN). Mice homozygous for spontaneous mutation of the leptin receptor (Leprdb) (BKS.Cg-m+/+ Leprdb/J or db/db; stock 000642; age, 12 weeks old) and their respective non-diabetic lean control littermates (db/+ ;age, 12 weeks old) were procured from the Jackson Laboratory (Bar Harbor, ME). A splinted full thickness excisional wound model was employed as described previously(Das et al., 2016, Ganesh et al., 2012). Briefly, the dorsal side of the mice was shaved, depilated and cleaned using betadine under anesthesia. Two 6-mm diameter full thickness (skin and panniculus carnosus)

excisional wounds were made on the dorsal skin with a 6-mm disposable biopsy punch(Das et al., 2016, Ganesh et al., 2012). A donut-shaped splint with an 8-mm inner diameter was made from an 0.5-mm thick silicone sheet (Grace Bio-Laboratories, Bend, OR) and placed on the wound using an immediate-bonding adhesive, followed by interrupted 5-0 nylon sutures (Ethicon, Somerville, NJ), such that the wound was centered within the splint(Das et al., 2016, Ganesh et al., 2012). The wound was covered with semi-occlusive dressing (Tegaderm™; 3M, St. Paul, MN). For effective topical recombinant mouse OSM (R&D Systems, Minneapolis, MN) application, the protein solution was injected under the Tegaderm™. This approach has effectively delivered recombinant protein delivery to mice excisional wounds(Das et al., 2016, Ganesh et al., 2012). Wound imaging was performed at specified times using a digital camera and the wound area was determined using Image J software(Das et al., 2016, Ganesh et al., 2012). The animals were euthanized at specific times and wound tissues were harvested for molecular and histological analysis.

Cell Culture

Human immortalized keratinocytes (HaCaT; provided kindly by Dr. NE Fusenig of German Cancer Research Center, Heidelberg, Germany) were grown under standard culture conditions as previously described(Banerjee et al., 2014, Biswas et al., 2010, Khandelwal et al., 2021). For inducing hyperglycemia, an additional 30mM D-glucose (Sigma-Aldrich, St. Louis, MO) was added to the media. L-glucose (additional 30mM; Sigma-Aldrich, St. Louis, MO; added to the media) served as osmolarity control.

Promoter Reporter Assay

Human immortalized keratinocytes (HaCaT) were transfected with p63 promoter reporter plasmid (HPRM34518; Genecopoeia, Rockville, MD). Luciferase assays were performed using Gaussian luciferase reporter assay (Genecopoeia, Rockville, MD). Normalization was achieved by SEAP value. Data were presented as ratio of Gaussian luciferase to secreted alkaline phosphatase(Sinha et al., 2018).

siRNA delivery to HaCaT cells

Transfection of HaCaT cells was performed as described(Biswas et al., 2010). Briefly, HaCaT cells were seeded in antibiotic-free DMEM medium 24h before transfection. DharmaFECT 1 transfection reagent (Dharmacon; Lafayette, CO) was used to transfect cells with 100 nmol/L siRNA smart pool, (Dharmacon; Lafayette, CO). Transfection of non-targeting siRNA negative controls was performed for the control groups. Cells were harvested/reseeded after 72h.

Immunohistochemistry (IHC) and Immunocytochemistry (ICC)

Immunostaining of p63, K14, ITGB1 and Ki67 was performed on cryosections of wound tissue samples or HaCaT cells using specific antibodies as described previously(Das et al., 2018, Ghosh et al., 2020, Sinha et al., 2018). For wound tissues, 10 μm thick cryosectioned tissues were fixed with cold acetone, blocked with 10% normal goat serum and incubated with specific antibodies against p63 (Cat# ab53039, Abcam, Cambridge, MA), K14 (Cat#

905304, Biolegend, San Diego, CA), ITGB1 (Cat# ab95623, Abcam, Cambridge, MA) and Ki67 (Cat# ab16667, Abcam, Cambridge, MA) overnight at 4°C.

For immunocytochemistry, HaCaT were fixed with Intracellular (IC) Fixation Buffer (eBioscience, San Diego, CA), permeabilized, blocked with 10% normal goat serum and incubated with specific antibodies against p63 (Cat# ab53039, Abcam, Cambridge, MA) and ITGB1 (Cat# ab134179, Abcam, Cambridge, MA) overnight at 4°C. Signal was visualized by subsequent incubation with fluorescence-tagged secondary antibodies followed by counterstaining with DAPI(Das et al., 2019, Khandelwal et al., 2021). Images were captured by Axioscanner microscope. Confocal microscopy was performed on a Zeiss LSM 880 microscope equipped with the AIRYscan detector(Scipioni et al., 2018). Quantification of fluorescent intensity of image was performed using ZenBlue (Zeiss, Germany) software. Wound re-epithelialization was calculated using ZenBlue (Zeiss, Germany) software by measuring the original width of the wound (W) and then measuring the portions of the wound that had re-epithelialized (E). Percent-re-epithelialized was calculated as: (E/W) × 100 as previously described(Roy et al., 2009).

ELISA

Levels of OSM (R & D Systems, Minneapolis, MN) were measured using commercially available ELISA kits(Das et al., 2019, Das et al., 2018, Das et al., 2016, Ganesh et al., 2012). pSTAT3 and STAT3 were measured from cell lysates measured using commercially available ELISA kit (Abcam, Cambridge, MA).

Laser capture microdissection (LCM)

Laser microdissection and pressure catapulting was carried out using the Microlaser system from PALM Microlaser Technologies AG (Zeiss, Germany). Briefly, OCT embedded wound tissues were cut into 10μm sections using a cryo-microtome. The cut sections were then placed on polyethylene napthalate membrane glass slides (P.A.L.M. Microlaser Technologies AG, Germany). Prior to use the membrane glass slides were treated with RNasin (Promega, Madison, WI) and UV-treated. The tissue sections were then cut and catapulted as described previously. Epithelial tissues visualized by H & E staining were captured in lysis buffer provided with Cells-Direct RNA kit (Invitrogen, Carlsbad, CA). This was followed by reverse transcription and mRNA quantification using real-time PCR(Sinha et al., 2018).

RNA extraction, reverse transcription and quantitative RT-PCR

mirVana RNA isolation kit (ThermoFisher, Waltham, MA) was used according to the manufacturer's instructions to extract total RNA as previously described(Chen and Benveniste, 2004). Quantification of mRNA was done by real-time or quantitative (Q)PCR assay using double-stranded DNA binding dye SYBR Green-I and primers specific for selected genes (Supplementary Table S3) as described previously(Das et al., 2018, Das et al., 2014, Ganesh et al., 2012). *18S* or *β-ACTIN* were used as reference housekeeping genes.

Western blot

Western blot was performed using primary antibodies against p63 (Cat# ab53039, Abcam, Cambridge, MA) and ITGB1 (Cat# ab134179, Abcam, Cambridge, MA) as described previously (Das et al., 2014, Das et al., 2016). Signal was visualized using corresponding HRP-conjugated secondary antibody and ECL Plus™ Western Blotting Detection Reagents (Thomas Scientific, Swedesboro, NJ). β-ACTIN (Cat# A5441, Sigma-Aldrich, St. Louis, MO) served as loading control. Image J (NIH) software was used for quantification of bands by densitometry analysis.

Immunoprecipitation

Immunoprecipitation (IP) of OSM was done using Dynabeads™ Protein G (ThermoFisher, Waltham, MA), according to the manufacturer's instructions and as previously described(Singh et al., 2019). Antibody binding to the Dynabeads™ magnetic beads was performed by incubating the beads with OSM antibody (Cat# sc-374039, Santa Cruz Biotechnology, Dallas, TX) 3h at room temperature. Wound-edge tissue lysates of diabetic animals were incubated with antibody bound to the bead overnight in a rotisserie shaker at 4°C to immunoprecipitate OSM. The beads were then washed three times with ice-cold lysis buffer, and the immunoprecipitated complexes were washed four times with lysis buffer. For Western blot, the IP samples were subjected to SDS-PAGE after reduction with 1M DTT, as previously described(Das et al., 2014, Das et al., 2016), and probed with anti-AGE Ab (Cat# ab23722, Abcam, Cambridge, MA). The membrane was stripped and reprobed with anti–OSM Ab (Cat# sc-374039, Santa Cruz Biotechnology, Dallas, TX). TrueBlot® secondary antibodies (Rockland Immunochemicals Inc. Pottstown, PA) were used for unhindered detection of blotted protein band of interest.

Cell Proliferation Assay

Cell proliferation assay was performed using CyQUANT cell proliferation assay kit (Invitrogen, Carlsbad, CA) as previously described(Biswas et al., 2010, Bureta et al., 2019, Guiducci et al., 2005).

Cell Migration assay

A cell migration assay was performed using culture inserts (IBIDI, Verona, WI) according to the manufacturer's instructions. Briefly, the cells were seeded in the chambers in such a way that a confluent monolayer is formed in the presence of the insert. Prior to the assay cells were treated with Mitomycin C (10μg/ml; 2h)(Grada et al., 2017, Sun et al., 2019). Removal of the insert generated a gap in the monolayer. Migration of cells across that gap was studied using time-lapse microscopy. Cell migration was measured using phase-contrast microscopy following withdrawal of the insert(Banerjee et al., 2014). Images were analyzed using the Zen Blue software.

OSM glycation

For glycation of OSM, 1μg human rOSM (R & D Systems, Minneapolis, MN) was treated with 12.5mM methylglyoxal (MGO) (Sigma-Aldrich; St. Louis, MO) with/without aminoguanidine hydrochloride (AG, 25mM) (Sigma-Aldrich; St. Louis, MO) at 37°C for

5 days. The glycation of OSM was determined using Methylglyoxal (MG) Competitive ELISA (Cell Biolabs, San Diego CA) as per manufacturer's instructions.

Data collection and statistical analyses

Data are reported as mean ± SEM of 3–8 experiments as indicated in respective figure legends. For human wound fluid studies, data from human subjects have been presented (Supplementary Tables 1 and 2). Student's t-test was used to determine significant differences between the means. Comparisons among multiple groups were tested using ANOVA (using Tukey's test for post hoc analysis). $p<0.05$ was considered statistically significant.

Supplementary Material

Refer to Web version on PubMed Central for supplementary material.

Acknowledgements

Human immortalized keratinocytes (HaCaT) was provided kindly by Dr. NE Fusenig of German Cancer Research Center, Heidelberg, Germany. Technical help from Dr. Kasturi Ganesh Barki, Piya Das Ghatak and Dr. Pradipta Banerjee is acknowledged for IHC sample processing and LCM capture. Some of the study materials used in this study were per MTA with The Ohio State University (OSU). Some of the authors including the first & corresponding authors were employees of OSU where part of the work was performed. This work was supported by the National Institutes of Health grants U01DK119099 and R01GM108014 to C.K.S., R01NR015676 to C.K.S. and S.R. and R01DK114718 to S.R.

Data availability Statement

No datasets were generated or analyzed during the current study.

Abbreviations

OSM	Oncostatin M
TP63	tumor protein 63
ITGB1	integrin beta 1
JAK	Janus kinase
STAT	signal transducer and activation transcription
MGO	methyl gloxal
AG	aminoguanidine

References

Banerjee J, Das Ghatak P, Roy S, Khanna S, Sequin EK, Bellman K, et al. Improvement of human keratinocyte migration by a redox active bioelectric dressing. PLoS One 2014;9(3):e89239. [PubMed: 24595050]

Beigel F, Friedrich M, Probst C, Sotlar K, Goke B, Diegelmann J, et al. Oncostatin M mediates STAT3-dependent intestinal epithelial restitution via increased cell proliferation, decreased

apoptosis and upregulation of SERPIN family members. PLoS One 2014;9(4):e93498. [PubMed: 24710357]

Biswas S, Roy S, Banerjee J, Hussain SR, Khanna S, Meenakshisundaram G, et al. Hypoxia inducible microRNA 210 attenuates keratinocyte proliferation and impairs closure in a murine model of ischemic wounds. Proc Natl Acad Sci U S A 2010;107(15):6976–81. [PubMed: 20308562]

Boniface K, Diveu C, Morel F, Pedretti N, Froger J, Ravon E, et al. Oncostatin M secreted by skin infiltrating T lymphocytes is a potent keratinocyte activator involved in skin inflammation. J Immunol 2007;178(7):4615–22. [PubMed: 17372020]

Bureta C, Setoguchi T, Saitoh Y, Tominaga H, Maeda S, Nagano S, et al. TGF-beta Promotes the Proliferation of Microglia In Vitro. Brain Sci 2019;10(1).

Canady J, Arndt S, Karrer S, Bosserhoff AK. Increased KGF expression promotes fibroblast activation in a double paracrine manner resulting in cutaneous fibrosis. J Invest Dermatol 2013;133(3):647–57. [PubMed: 23096718]

Chen SH, Benveniste EN. Oncostatin M: a pleiotropic cytokine in the central nervous system. Cytokine Growth Factor Rev 2004;15(5):379–91. [PubMed: 15450253]

Das A, Abas M, Biswas N, Banerjee P, Ghosh N, Rawat A, et al. A Modified Collagen Dressing Induces Transition of Inflammatory to Reparative Phenotype of Wound Macrophages. Sci Rep 2019;9(1):14293. [PubMed: 31586077]

Das A, Datta S, Roche E, Chaffee S, Jose E, Shi L, et al. Novel mechanisms of Collagenase Santyl Ointment (CSO) in wound macrophage polarization and resolution of wound inflammation. Sci Rep 2018;8(1):1696. [PubMed: 29374192]

Das A, Ganesh K, Khanna S, Sen CK, Roy S. Engulfment of apoptotic cells by macrophages: a role of microRNA-21 in the resolution of wound inflammation. J Immunol 2014;192(3):1120–9. [PubMed: 24391209]

Das A, Ghatak S, Sinha M, Chaffee S, Ahmed NS, Parinandi NL, et al. Correction of MFG-E8 Resolves Inflammation and Promotes Cutaneous Wound Healing in Diabetes. J Immunol 2016;196(12):5089–100. [PubMed: 27194784]

DiPersio CM, Zheng R, Kenney J, Van De Water L. Integrin-mediated regulation of epidermal wound functions. Cell Tissue Res 2016;365(3):467–82. [PubMed: 27351421]

Fossey SL, Bear MD, Kisseberth WC, Pennell M, London CA. Oncostatin M promotes STAT3 activation, VEGF production, and invasion in osteosarcoma cell lines. BMC Cancer 2011;11:125. [PubMed: 21481226]

Gadient RA, Patterson PH. Leukemia inhibitory factor, Interleukin 6, and other cytokines using the GP130 transducing receptor: roles in inflammation and injury. Stem Cells 1999;17(3):127–37. [PubMed: 10342555]

Ganesh K, Das A, Dickerson R, Khanna S, Parinandi NL, Gordillo GM, et al. Prostaglandin E(2) induces oncostatin M expression in human chronic wound macrophages through Axl receptor tyrosine kinase pathway. J Immunol 2012;189(5):2563–73. [PubMed: 22844123]

Ghosh N, Das A, Biswas N, Gnyawali S, Singh K, Gorain M, et al. Urolithin A augments angiogenic pathways in skeletal muscle by bolstering NAD+ and SIRT1. Scientific Reports 2020;in press.

Gladden LB. Lactate metabolism: a new paradigm for the third millennium. J Physiol 2004;558(Pt 1):5–30. [PubMed: 15131240]

Gomez-Lechon MJ. Oncostatin M: signal transduction and biological activity. Life Sci 1999;65(20):2019–30. [PubMed: 10579456]

Goren I, Kampfer H, Muller E, Schiefelbein D, Pfeilschifter J, Frank S. Oncostatin M expression is functionally connected to neutrophils in the early inflammatory phase of skin repair: implications for normal and diabetes-impaired wounds. J Invest Dermatol 2006;126(3):628–37. [PubMed: 16410783]

Grada A, Otero-Vinas M, Prieto-Castrillo F, Obagi Z, Falanga V. Research Techniques Made Simple: Analysis of Collective Cell Migration Using the Wound Healing Assay. J Invest Dermatol 2017;137(2):e11–e6. [PubMed: 28110712]

Grose R, Hutter C, Bloch W, Thorey I, Watt FM, Fassler R, et al. A crucial role of beta 1 integrins for keratinocyte migration in vitro and during cutaneous wound repair. Development 2002;129(9):2303–15. [PubMed: 11959837]

Guiducci S, Del Rosso A, Cinelli M, Perfetto F, Livi R, Rossi A, et al. Raloxifene reduces urokinase-type plasminogen activator-dependent proliferation of synoviocytes from patients with rheumatoid arthritis. Arthritis Res Ther 2005;7(6):R1244–53. [PubMed: 16277677]

Houben E, Hellings N, Broux B. Oncostatin M, an Underestimated Player in the Central Nervous System. Front Immunol 2019;10:1165. [PubMed: 31191538]

Hunt TK, Aslam RS, Beckert S, Wagner S, Ghani QP, Hussain MZ, et al. Aerobically derived lactate stimulates revascularization and tissue repair via redox mechanisms. Antioxid Redox Signal 2007;9(8):1115–24. [PubMed: 17567242]

Jorcyk CL, Holzer RG, Ryan RE. Oncostatin M induces cell detachment and enhances the metastatic capacity of T-47D human breast carcinoma cells. Cytokine 2006;33(6):323–36. [PubMed: 16713283]

Khandelwal P, Das A, Sen CK, Srinivas SP, Roy S, Khanna S. A surfactant polymer wound dressing protects human keratinocytes from inducible necroptosis. Sci Rep 2021;11(1):4357. [PubMed: 33623080]

Koivisto L, Heino J, Hakkinen L, Larjava H. Integrins in Wound Healing. Adv Wound Care (New Rochelle) 2014;3(12):762–83. [PubMed: 25493210]

Koster MI, Dai D, Marinari B, Sano Y, Costanzo A, Karin M, et al. p63 induces key target genes required for epidermal morphogenesis. Proc Natl Acad Sci U S A 2007;104(9):3255–60. [PubMed: 17360634]

Koster MI, Roop DR. The role of p63 in development and differentiation of the epidermis. J Dermatol Sci 2004;34(1):3–9. [PubMed: 14757276]

Kuzuya M, Satake S, Ai S, Asai T, Kanda S, Ramos MA, et al. Inhibition of angiogenesis on glycated collagen lattices. Diabetologia 1998;41(5):491–9. [PubMed: 9628264]

Leibovich SJ, Ross R. The role of the macrophage in wound repair. A study with hydrocortisone and antimacrophage serum. Am J Pathol 1975;78(1):71–100. [PubMed: 1109560]

McCarty SM, Percival SL. Proteases and Delayed Wound Healing. Adv Wound Care (New Rochelle) 2013;2(8):438–47. [PubMed: 24688830]

Mirza R, DiPietro LA, Koh TJ. Selective and specific macrophage ablation is detrimental to wound healing in mice. Am J Pathol 2009;175(6):2454–62. [PubMed: 19850888]

Morasso MI, Tomic-Canic M. Epidermal stem cells: the cradle of epidermal determination, differentiation and wound healing. Biol Cell 2005;97(3):173–83. [PubMed: 15715523]

Morita K, Urabe K, Moroi Y, Koga T, Nagai R, Horiuchi S, et al. Migration of keratinocytes is impaired on glycated collagen I. Wound Repair Regen 2005;13(1):93–101. [PubMed: 15659041]

Nguyen TN, Rajapakshe K, Nicholas C, Tordesillas L, Ehli EA, Davis CM, et al. Integrative transcriptomic analysis for linking acute stress responses to squamous cell carcinoma development. Sci Rep 2020;10(1):17209. [PubMed: 33057049]

Pastar I, Stojadinovic O, Yin NC, Ramirez H, Nusbaum AG, Sawaya A, et al. Epithelialization in Wound Healing: A Comprehensive Review. Adv Wound Care (New Rochelle) 2014;3(7):445–64. [PubMed: 25032064]

Peppa M, Stavroulakis P, Raptis SA. Advanced glycoxidation products and impaired diabetic wound healing. Wound Repair Regen 2009;17(4):461–72. [PubMed: 19614910]

Romano RA, Smalley K, Magraw C, Serna VA, Kurita T, Raghavan S, et al. DeltaNp63 knockout mice reveal its indispensable role as a master regulator of epithelial development and differentiation. Development 2012;139(4):772–82. [PubMed: 22274697]

Roy S, Biswas S, Khanna S, Gordillo G, Bergdall V, Green J, et al. Characterization of a preclinical model of chronic ischemic wound. Physiol Genomics 2009;37(3):211–24. [PubMed: 19293328]

Ryan RE, Martin B, Mellor L, Jacob RB, Tawara K, McDougal OM, et al. Oncostatin M binds to extracellular matrix in a bioactive conformation: implications for inflammation and metastasis. Cytokine 2015;72(1):71–85. [PubMed: 25622278]

Santamaria M, Pardo-Saganta A, Alvarez-Asiain L, Di Scala M, Qian C, Prieto J, et al. Nuclear alpha1-antichymotrypsin promotes chromatin condensation and inhibits proliferation of human hepatocellular carcinoma cells. Gastroenterology 2013;144(4):818–28 e4. [PubMed: 23295442]

Scipioni L, Lanzano L, Diaspro A, Gratton E. Comprehensive correlation analysis for super-resolution dynamic fingerprinting of cellular compartments using the Zeiss Airyscan detector. Nat Commun 2018;9(1):5120. [PubMed: 30504919]

Shin SH, Han SK, Jeong SH, Kim WK. Potential of oncostatin M to accelerate diabetic wound healing. Int Wound J 2014;11(4):398–403. [PubMed: 23116288]

Singh K, Sinha M, Pal D, Tabasum S, Gnyawali SC, Khona D, et al. Cutaneous Epithelial to Mesenchymal Transition Activator ZEB1 Regulates Wound Angiogenesis and Closure in a Glycemic Status-Dependent Manner. Diabetes 2019;68(11):2175–90. [PubMed: 31439646]

Sinha M, Sen CK, Singh K, Das A, Ghatak S, Rhea B, et al. Direct conversion of injury-site myeloid cells to fibroblast-like cells of granulation tissue. Nat Commun 2018;9(1):936. [PubMed: 29507336]

Sterbova S, Karlsson T, Persson E. Oncostatin M induces tumorigenic properties in non-transformed human prostate epithelial cells, in part through activation of signal transducer and activator of transcription 3 (STAT3). Biochem Biophys Res Commun 2018;498(4):769–74. [PubMed: 29526757]

Stojadinovic O, Brem H, Vouthounis C, Lee B, Fallon J, Stallcup M, et al. Molecular pathogenesis of chronic wounds: the role of beta-catenin and c-myc in the inhibition of epithelialization and wound healing. Am J Pathol 2005;167(1):59–69. [PubMed: 15972952]

Sun L, Jin X, Xie L, Xu G, Cui Y, Chen Z. Swainsonine represses glioma cell proliferation, migration and invasion by reduction of miR-92a expression. BMC Cancer 2019;19(1):247. [PubMed: 30890138]

Takahashi M Glycation of Proteins. In: Taniguchi N, Endo T, Hart GW, Seeberger PH, Wong C-H, editors. Glycoscience: Biology and Medicine. Tokyo: Springer Japan; 2015. p. 1339–45.

Thornalley PJ. Use of aminoguanidine (Pimagedine) to prevent the formation of advanced glycation endproducts. Arch Biochem Biophys 2003;419(1):31–40. [PubMed: 14568006]

Truong AB, Kretz M, Ridky TW, Kimmel R, Khavari PA. p63 regulates proliferation and differentiation of developmentally mature keratinocytes. Genes Dev 2006;20(22):3185–97. [PubMed: 17114587]

Wautier JL, Schmidt AM. Protein glycation: a firm link to endothelial cell dysfunction. Circ Res 2004;95(3):233–8. [PubMed: 15297385]

Wooten DK, Xie X, Bartos D, Busche RA, Longmore GD, Watowich SS. Cytokine signaling through Stat3 activates integrins, promotes adhesion, and induces growth arrest in the myeloid cell line 32D. J Biol Chem 2000;275(34):26566–75. [PubMed: 10858439]

Yu PH, Zuo DM. Aminoguanidine inhibits semicarbazide-sensitive amine oxidase activity: implications for advanced glycation and diabetic complications. Diabetologia 1997;40(11):1243–50. [PubMed: 9389414]

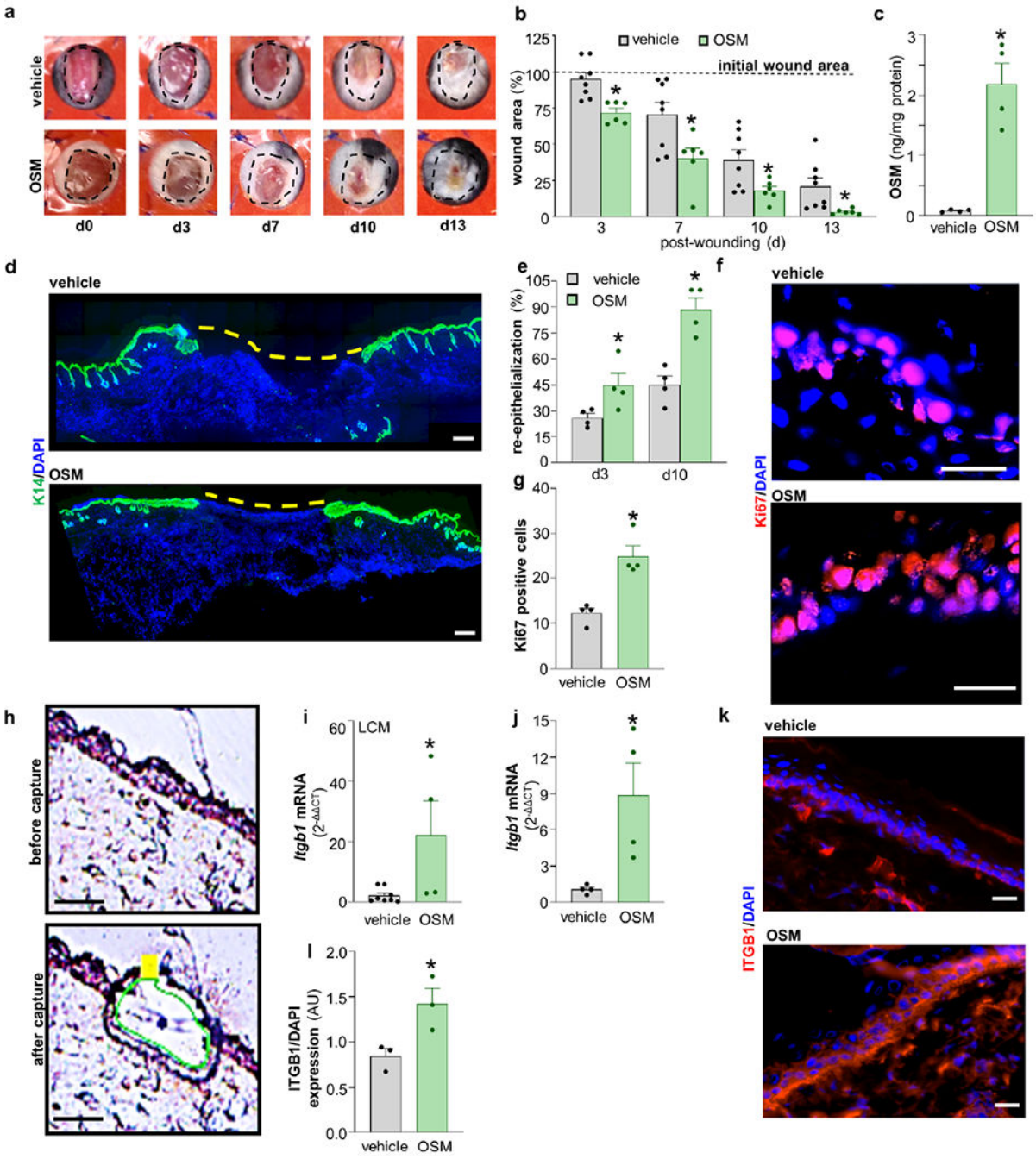

Figure 1. OSM treatment to murine wounds accelerates wound closure by increased re-epithelialization.

Full-thickness (skin and panniculus carnosum) dorsal wounds were created on the male C57bl/6 mice by using a 6-mm biopsy punch. The wounds were stented and treated with recombinant mouse OSM (1.25 μg.15μl^{-1}.wound^{-1}). Control wounds received vehicle only. Wounds were imaged on d0–13 post-wounding. Wound areas were calculated using digital planimetry. **(a)** Representative digital images of wounds from OSM and vehicle-treated mice d0–13 post-wounding. **(b)** Wound closure kinetics. Data are expressed as mean ± SEM (n =

6-8). *p<0.05 compared with vehicle-treated wounds. **(c)** OSM levels on d13 post-wounding in wounds tissue treated with recombinant OSM. Data are expressed as mean ± SEM (n = 4). *p<0.05 compared with vehicle-treated. **(d)** Representative images of K14-stained d3 wound tissues. Yellow dotted lines represent the non-re-epithelialized region. Scale bar, 200μm. **(e)** Wound re-epithelialization calculated on d3 and d10 post-wounding. Data are expressed as mean ± SEM (n=4). *p;<0.05 compared with vehicle-treated wounds. **(f, g)** Representative images and quantification and of d3 wound-edge tissue sections from OSM-treated mice stained with Ki67 (red) and counterstained with DAPI (blue, nuclear). Scale bar, 20μm. Data are expressed as mean ± SEM (n = 4) in the field of view. *p<0.05 compared with vehicle-treated wounds. **(h)** Laser capture micro-dissected (LCM) epithelial cells from full thickness excisional wounds. Scale bar, 37.5μm. **(i)** mRNA expression of *Itgb1* in LCM-captured wound–edge keratinocytes from d3 wounds of OSM-treated mice. Data are expressed as mean ± SEM (n = 4-8). *p<0.05 compared with vehicle-treated wounds. **(j)** mRNA expression of *Itgb1* in wound–edge tissues from OSM-treated mice. Data are expressed as mean ± SEM (n = 4). *p;<0.05 compared with vehicle-treated wounds. **(k, l)** Representative images and quantification and of d3 wound-edge tissue sections from OSM-treated mice stained with ITGB1 (red) and counterstained with DAPI (blue, nuclear). Scale bar, 20μm. Data are expressed as mean ± SEM (n = 3). *p<0.05 compared with vehicle-treated wounds.

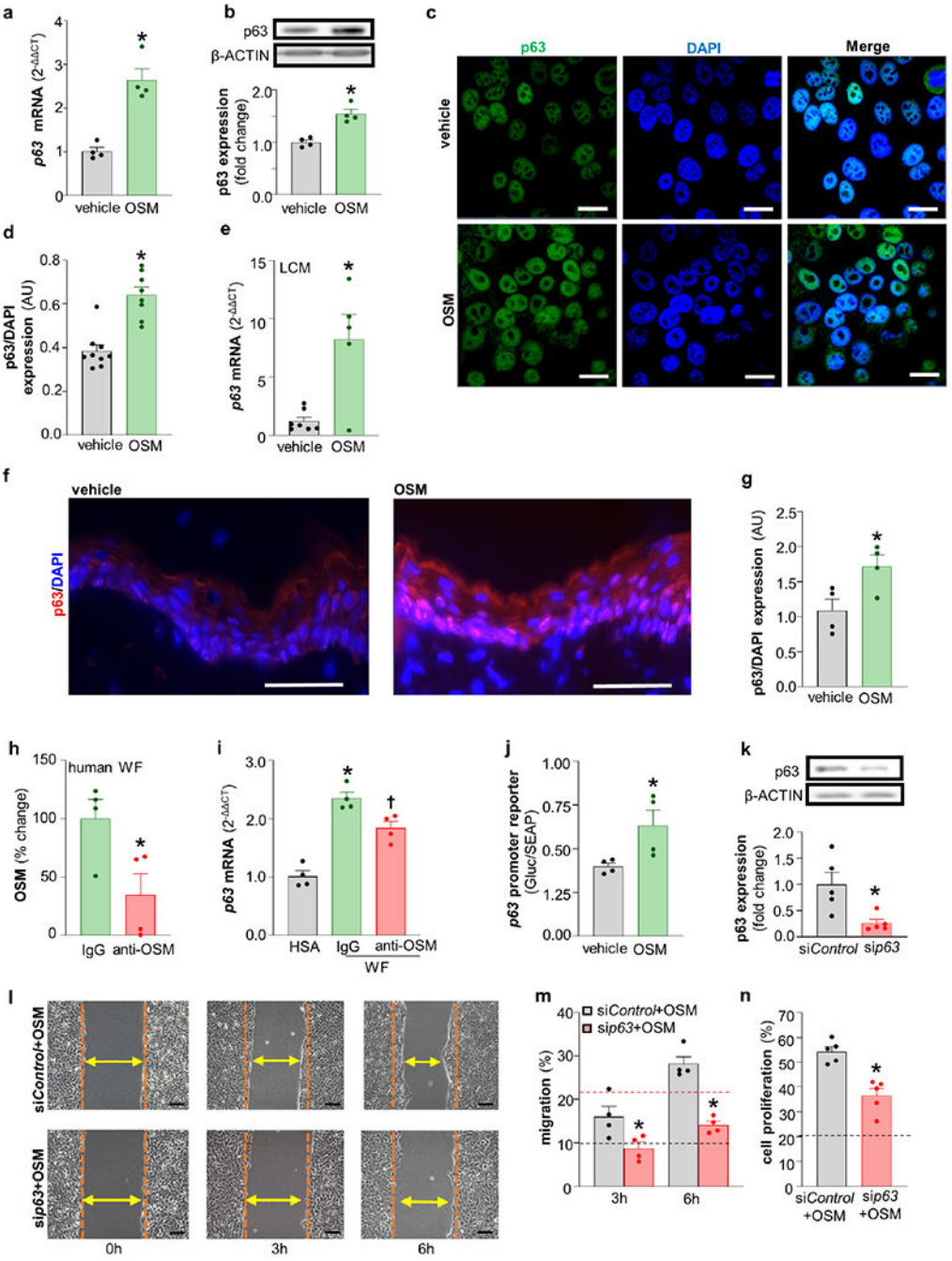

Figure 2. OSM induces p63 in the wound-edge epithelium and keratinocytes

(a-d) Human HaCaT keratinocytes were treated with recombinant OSM (25ng/ml) for 72h. **(a)** *p63* mRNA expression was measured using RT-PCR. Data are expressed as mean ± SEM (n=4). *p<0.05 compared with vehicle. **(b)** p63 protein expression was measured using Western blot. β-ACTIN was used as a loading control. Representative blot from four independent experiments has been provided. Densitometry quantification of band intensity has been presented. Data are expressed as mean ± SEM (n = 4). *p<0.05 compared with vehicle. **(c, d)** p63 protein expression was measured using immunocytochemistry.

Scale bar, 20μm. Data are expressed as mean ± SEM (n = 8-9). *p<0.05 compared with vehicle. **(e-g)** Full-thickness (skin and panniculus carnosum) dorsal wounds were created on the male C57bl/6 mice by using a 6-mm biopsy punch. The wounds were stented and treated with recombinant mouse OSM (1.25 μg.15μl^{-1}.wound^{-}). Control wounds received vehicle only. **(e)** *p63* mRNA expression in LCM-captured wound-edge keratinocytes from d3 wounds of OSM-treated mice. Data are expressed as mean ± SEM (n = 5-7). *p<0.05 compared with vehicle-treated wounds. **(f)** Representative images of d3 wound-edge tissue sections from OSM-treated mice stained with p63 (red) and counterstained with DAPI (blue, nuclear). Scale bar, 50μm. **(g)** Quantification of p63 on d3 post-wounding. Data are expressed as mean ± SEM (n = 4). *p<0.05 compared with vehicle-treated wounds. **(h)** OSM in human wound fluid (see Supplementary Table 1 for subject demographics) was neutralized with OSM neutralizing antibody (1 μg/ml) for 4h and subjected to ELISA to check the levels of OSM. Data are expressed as mean ± SEM (n = 5). *p<0.05 compared with IgG-treated wound fluids. **(i)** HaCaT cells were treated with OSM-neutralized wound fluid (10%v/v; 72h) and *p63* mRNA expression were measured using RT-PCR. Data are expressed as mean ± SEM (n = 3). *p<0.05 compared with human serum albumin (HSA) treated HaCaT cells. $^{\dagger}p$<0.05 compared with HaCaT cells exposed to IgG-treated wound fluids. **(j)** Human HaCaT keratinocytes were transfected with luciferase reporter vector pEZX-PG04 containing promoter for p63 upstream of secreted Gaussia luciferase (Gluc) and secreted alkaline phosphatase (SEAP, endogenous control), followed by treatment with OSM (25ng/ml, 72h). Luciferase activity measured as GLuc/SEAP. Data are expressed as mean ± SEM (n=4). *p<0.05 compared with vehicle. **(k-n)** Human HaCaT keratinocytes were transfected with si*p63* or si*Control*. **(k)** p63 protein expression was measured following knockdown of *p63* using siRNA for 72h. Data are expressed as mean ± SEM (n = 5). *p<0.05 compared with si*Control*. **(1, m)** Knockdown of *p63* in keratinocytes using siRNA was followed by treatment with OSM (25ng/ml; 72h) after which cells were subjected to migration assay. Migration of cells was observed at 3h and 6h following removal of inserts. Scale bar, 100μm. Black and red dotted line represents migration under similar conditions in presence of vehicle alone at 3h and 6h respectively. Data are expressed as mean ± SEM (n = 4). *p<0.05 compared with si*Control* treated with OSM. **(n)** Cells were activated with OSM (25ng/ml) for 72h after knockdown of *p63* in keratinocytes using siRNA. Cell proliferation was measured under low (0.2%) serum using CyQUANT. Black dotted line represents proliferation under similar conditions in presence of vehicle alone. Data are expressed as mean ± SEM (n = 5). *p<0.05 compared with si*Control* treated with OSM.

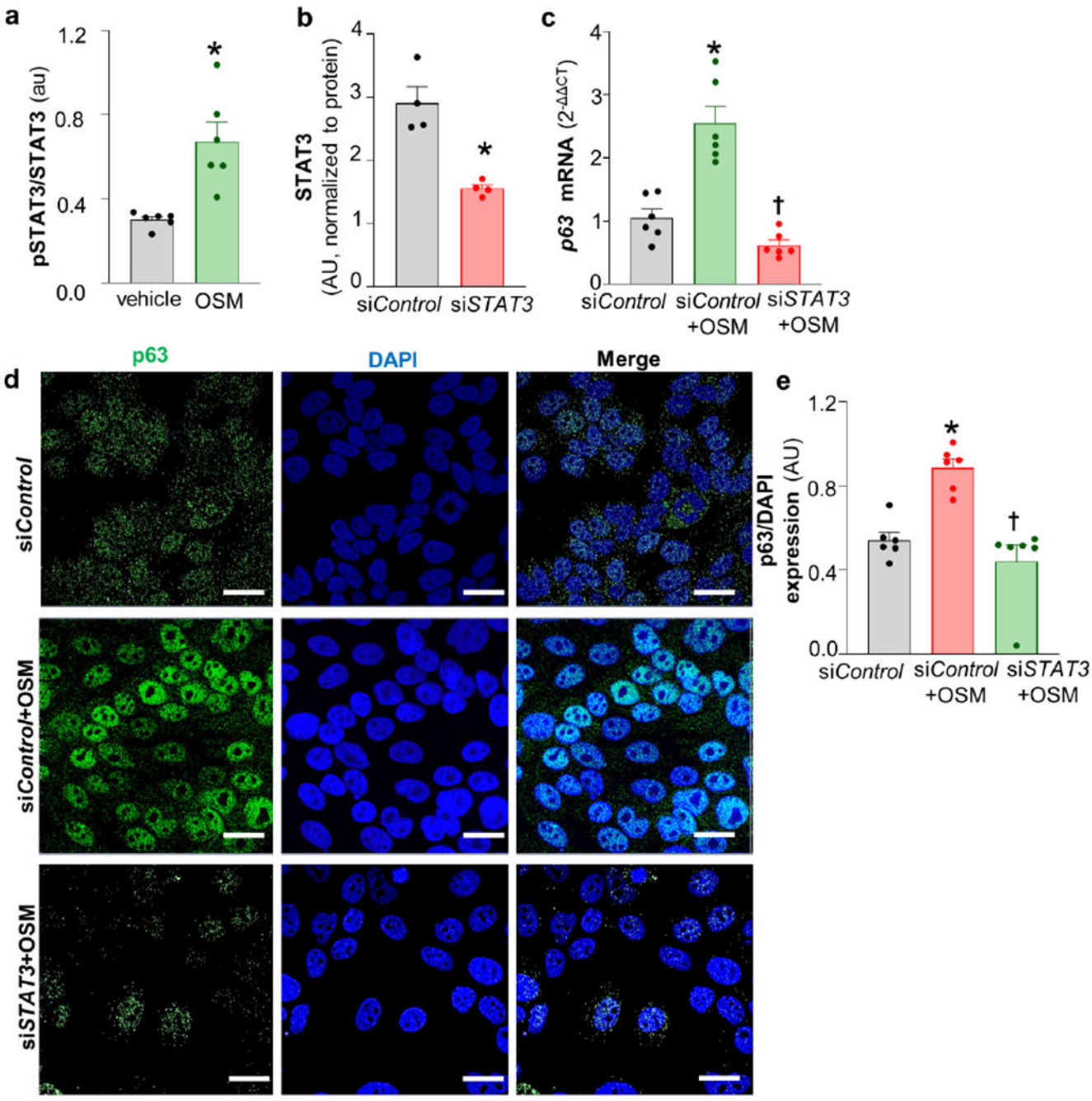

Figure 3. OSM induced p63 expression is mediated *via* STAT3.

(a) Human HaCaT keratinocytes were treated with recombinant OSM (25ng/ml) for 72h. pSTAT3/STAT3 was measured in the cell lysate using pSTAT3 and STAT3 ELISA kit. Data are expressed as mean ± SEM (n=6). *p<0.05 compared with vehicle **(b)** Human HaCaT keratinocytes were transfected with si*STAT3* or si*Control*. STAT3 was measured in the cell lysate using STAT3 ELISA kit. Data are normalized to total protein and expressed as mean ± SEM (n=4). *p<0.05 compared with si*Control*. **(c-e)** Human HaCaT keratinocytes were transfected with si*STAT3* or si*Control* followed by treatment with recombinant OSM

(25ng/ml; 72h). **(c)** *p63* mRNA expression was measured using RT-PCR. Data are expressed as mean ± SEM (n=6). *p<0.05 compared with si*Control*. †p0.05 compared with si*Control* treated with OSM. **(d, e)** p63 protein expression. was measured using immunocytochemistry. Scale bar, 20μm. Data are expressed as mean ± SEM (n=6). *p<0.05 compared with si*Control*. †p<0.05 compared with si*Control* treated with OSM.

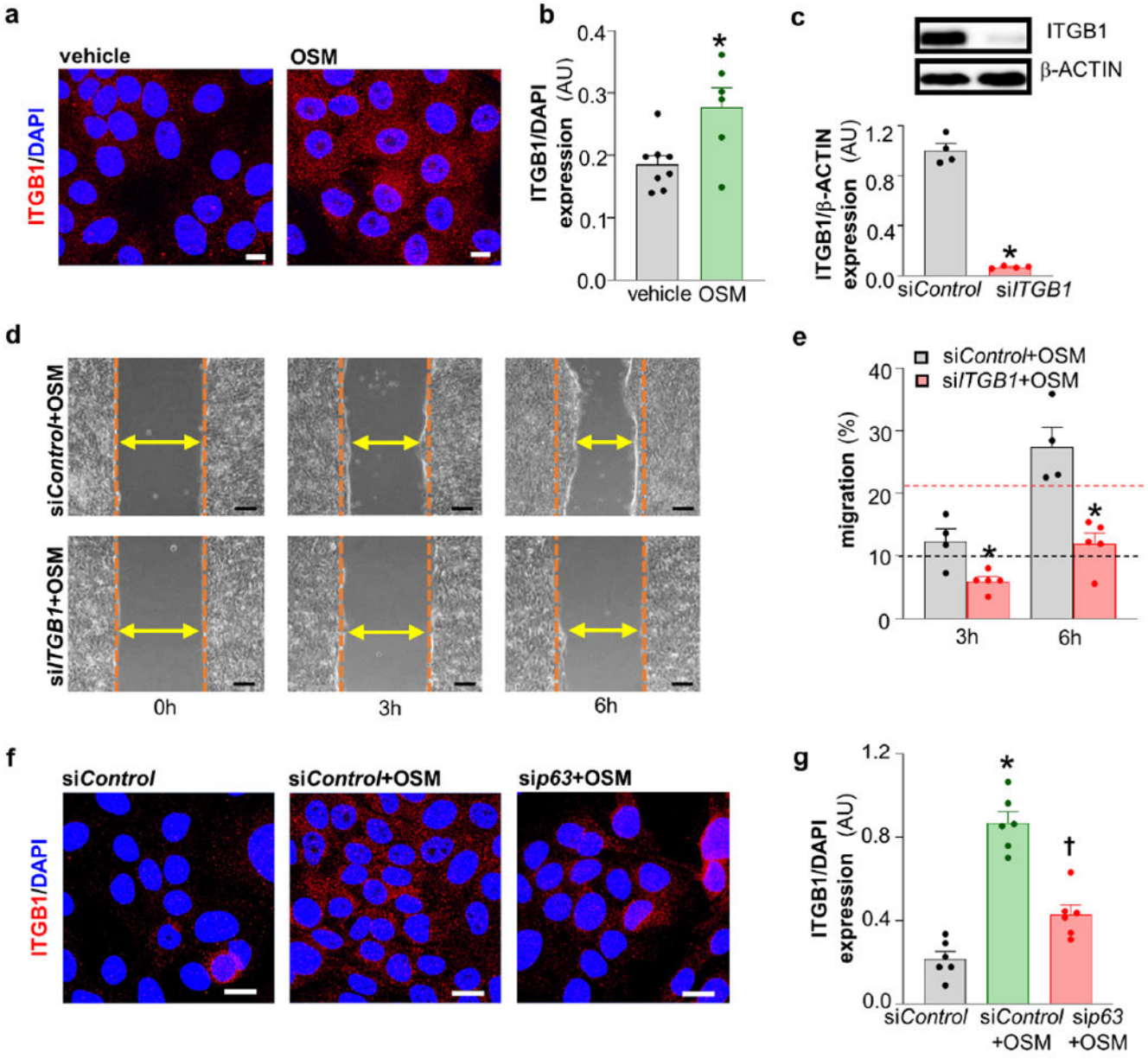

Figure 4. OSM induced ITGB1 expression through p63-mediated pathway.

(a, b) Human HaCaT keratinocytes were treated with recombinant OSM (25ng/ml) for 72h. ITGB1 protein expression was measured using immunocytochemistry. Scale bar, 10μm. Data are expressed as mean ± SEM (n = 6-8). *p<0.05 compared with vehicle. **(c)** ITGB1 protein expression was measured following knockdown of *ITGB1* using siRNA for 72h using Western Blot. β-ACTIN was used as a loading control. Data are expressed as mean ± SEM (n = 4). *p<0.05 compared with si*Control*. **(d, e)** Human HaCaT keratinocytes were transfected with si*ITGB1*or si*Control* followed by treatment with OSM (25ng/ml; 72h) after which cells were subjected to migration assay. Migration of cells was observed at 3h and 6h following removal of inserts. Scale bar, 100μm. Black and red dotted line represents migration under similar conditions in presence of vehicle alone at 3h and 6h respectively.

Data are expressed as mean ± SEM (n = 4-5). *p<0.05 compared with si*Control* treated with OSM. **(f, g)** Human HaCaT keratinocytes were transfected with si*p63* or si*Control*. Cells were activated with OSM (25ng/ml) for 72h after knockdown of *p63* in keratinocytes. ITGB1 protein expression was determined using immunocytochemistry. Scale bar, 20μm. Data are expressed as mean ± SEM (n = 6). *p<0.05 compared with si*Control*. $^{\dagger}p$<0.05 compared with si*Control* treated with OSM.

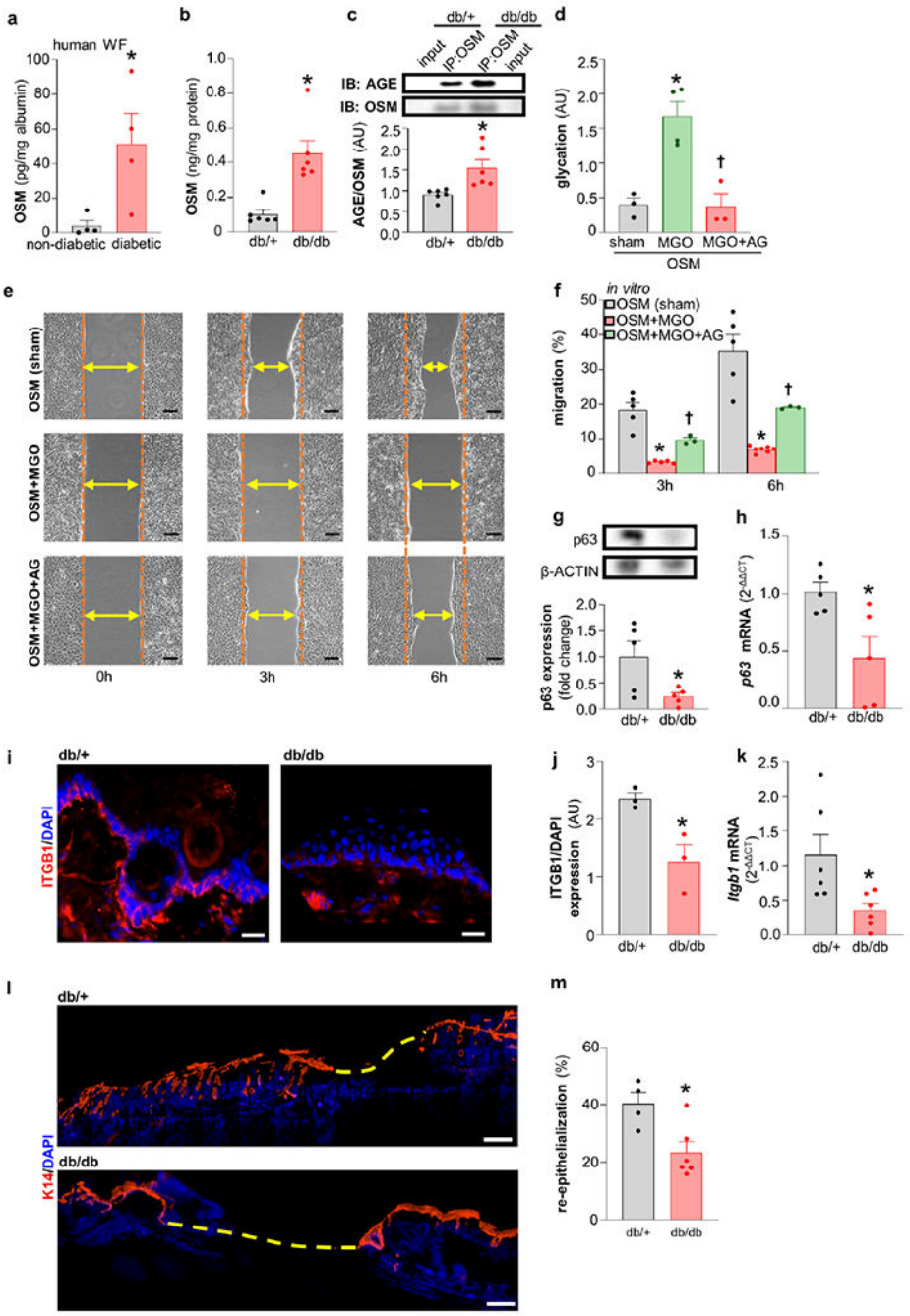

Figure 5. High levels of dysfunctional OSM in the diabetic wound environment results in impaired migration and re-epithelialization.

(a) Levels of OSM in wound fluid (WF) obtained from diabetic and non-diabetic chronic wounds (see Supplementary Table 2 for subject demographics). OSM levels were determined using ELISA and normalized to albumin. Data are mean ± SEM (n = 4). *$p<0.05$ compared with non-diabetic WF. **(b)** Full-thickness dorsal wounds were created using a 6-mm biopsy punch on dorsal side of diabetic (Leprdb, db/db) or corresponding non-diabetic controls (heterozygous, Leprdb/+, db/+) mice. The wounds were stented and left to heal by

secondary intention. OSM levels in d5 wound-edge tissue was determined using ELISA. Data are mean ± SEM (n = 6). *p<0.05 compared to db/+. **(c)** Immunoprecipitation (IP) of OSM from d5 wound-edge tissue lysates of diabetic (db/db) or corresponding non-diabetic controls (db/+) mice. The IP was subjected to SDS–PAGE followed by immunoblotting (IB) with anti-AGE antibody. Input represents cell lysates 5% of the lysate not subjected to immunoprecipitation reaction. Data are mean ± SEM (n = 6). *p<0.05 compared to db/+. **(d-f)** OSM was incubated with Methyl Glyoxal (MGO, 12.5mM, 5d) in presence of aminoguanidine hydrochloride (AG, 25mM, 5d). **(d)** Glycation was measured using Methylglyoxal Competitive ELISA kit. Data are expressed as mean ± SEM (n = 3-4). *p<0.05 compared with OSM (sham). $^{\dagger}p$<0.05 compared with OSM treated with MGO without AG. **(e, f)** The glycated OSM was used to treat human HaCaT keratinocytes (equivalent of 25ng/ml of OSM; 3d). Cells were then subjected to migration assay. Migration of cells was observed at 3h and 6h following removal of inserts. Scale bar, 100μm. Data are expressed as mean ± SEM (n = 3-7). *p<0.05 compared with cells treated with OSM (sham). $^{\dagger}p$<0.05 compared with cells treated with MGO-treated OSM without AG. **(g)** p63 protein expression in db/db wound-edge tissues was measured using Western Blot. β-ACTIN was used as a loading control. Representative blot from four independent experiments has been provided. Densitometry quantification of band intensity has been presented. Data are mean ± SEM (n = 5). *p<0.05 compared to db/+. **(h)***p63* mRNA expression in db/db wound-edge tissues. Data are mean ± SEM (n = 5). *p<0.05 compared to db/+. **(i, j)** Representative images and quantification of d5 wound-edge tissue sections from db/db and db/+ mice stained with ITGB1 (red) and counterstained with DAPI (blue, nuclear). Scale bar, 20μm. Data are mean ± SEM (n = 3). *p<0.05 compared to db/+. **(k)** *Itgb1* mRNA expression in db/db wound-edge tissues. Data are mean ± SEM (n = 6). *p<0.05 compared to db/+. **(l)** Representative images of K14-stained d7 wound tissues. Yellow dotted lines represent the non-re-epithelialized region. Scale bar, 500μm. **(m)** Wound re-epithelialization calculated on d7 post-wounding. Data are expressed as mean ± SEM (n = 4-6). *p<0.05 compared to db/+.

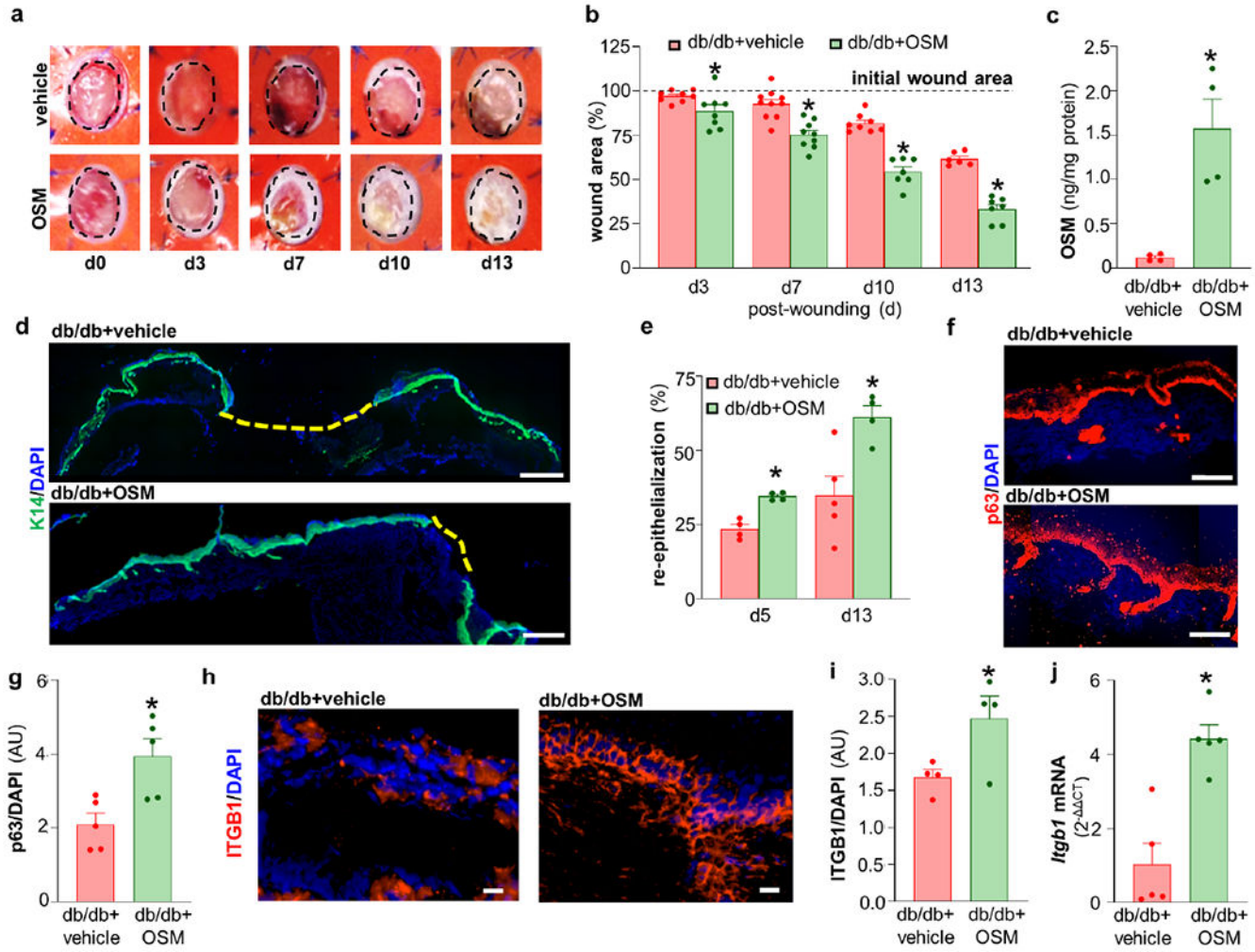

Figure 6. OSM treatment to diabetic murine wounds accelerates wound closure by increased re-epithelialization.

Full-thickness (skin and panniculus carnosum) dorsal wounds were created on the male db/db mice by using a 6-mm biopsy punch. The wounds were stented and treated with recombinant mouse OSM (1.25 μg.15μl^{-1}.wound^{-1}). Control wounds received vehicle only. Wounds were imaged on d0–13 post-wounding. Wound areas were calculated using digital planimetry. **(a, b)** Wound closure kinetics. Representative digital images of wounds from OSM and vehicle-treated mice d0–13 post-wounding. Data are expressed as mean ± SEM (n = 6-10). *p<0.05 compared with vehicle-treated wounds. **(c)** OSM levels on d13 post-wounding in diabetic wounds tissue treated with recombinant OSM. Data are expressed as mean ± SEM (n = 4). *p<0.05 compared with vehicle-treated wounds. **(d)** Representative images of K14-stained d13 wound tissues. Yellow dotted lines represent the non-re-epithelialized region. Scale bar, 1000μm. **(e)** Wound re-epithelialization calculated on d5 and d13 post-wounding. Data are expressed as mean ± SEM (n = 4-5). *p;<0.05 compared with vehicle-treated wounds. **(f-g)** Representative images and quantification of wound-edge tissue sections from OSM-treated db/db mice stained with p63 (red) and counterstained with DAPI (blue, nuclear). Scale bar, 200μm. Data are expressed as mean

± SEM (n = 5). *p<0.05 compared with vehicle-treated wounds. **(h-i)** Representative image and quantification of wound-edge tissue sections from OSM-treated db/db mice stained with ITGB1 (red) and counterstained with DAPI (blue, nuclear). Scale bar, 20μm. Data are expressed as mean ± SEM (n = 4). *p<0.05 compared with vehicle-treated wounds. **(j)** mRNA expression of *Itgb1* in wound–edge tissues from OSM-treated db/db mice. Data are expressed as mean ± SEM (n = 5). *p<0.05 compared with vehicle-treated wounds.